ORNL/TM-2017/136

PIE of Nuclear- Grade SiC/SiC Flexural Coupons Irradiated to 10 dpa at LWR Temperature

Nuclear Technology Research and Development

T. Koyanagi, Y. Katoh

Oak Ridge National Laboratory

Prepared for
U.S. Department of Energy
Campaign or Program

March 2017
M2FT-17OR020202101

ABSTRACT

Silicon carbide fiber-reinforced SiC matrix (SiC/SiC) composites are being actively investigated for accident-tolerant core structures of light water reactors (LWRs). Owing to the limited number of irradiation studies previously conducted at LWR-coolant temperature, this study examined SiC/SiC composites following neutron irradiation at 230–340°C to 2.0 and 11.8 dpa in the High Flux Isotope Reactor. The investigated materials are chemical vapor infiltrated (CVI) SiC/SiC composites with three different reinforcement fibers. The fiber materials were monolayer pyrolytic carbon (PyC)-coated Hi-Nicalon™ Type-S (HNS), Tyranno™ SA3 (SA3), and SCS-Ultra™ (SCS) SiC fibers. The irradiation resistance of these composites was investigated based on flexural behavior, dynamic Young's modulus, swelling, and microstructures. There was no notable mechanical properties degradation of the irradiated HNS and SA3 SiC/SiC composites except for reduction of the Young's moduli by up to 18%. The microstructural stability of these composites supported the absence of degradation. In addition, no progressive swelling from 2.0 to 11.8 dpa was confirmed for these composites. On the other hand, the SCS composite showed significant mechanical degradation associated with cracking within the fiber. This study determined that SiC/SiC composites with HNS or SA3 SiC/SiC fibers, a PyC interphase, and a CVI SiC matrix retain their properties beyond the lifetime dose for LWR fuel cladding at the relevant temperature.

INTENTIONALLY BLANK

CONTENTS

FIGURES

TABLES

ACKNOWLEDGMENTS

This research was supported by the United States Department of Energy (DOE) Office of Nuclear Energy for the Advanced Fuels Campaign of the Nuclear Technology R&D program under contact DE-AC05-00OR22725 with Oak Ridge National Laboratory (ORNL) managed by UT Battelle, LLC. A portion of this research used resources at the High Flux Isotope Reactor, a DOE Office of Science User Facility operated by ORNL. This work also used resources at the High Temperature Materials Laboratory at ORNL. The authors would like to thank Nesrin Cetiner at ORNL for design of the irradiation capsules and simulation of the irradiation temperature. The authors wish to thank Anne Campbell and Caen Ang at ORNL for valuable comments of this manuscript.

ACRONYMS

2D	two-dimensional
BF	bright field
CVD	chemically vapor deposited
CVI	chemical vapor infiltrated
DOE	Department of Energy
dpa	displacements per atom
FIB	focused ion beam
HAADF	high-angle annular dark field
HNS	Hi-Nicalon™ Type-S
LWR	light water reactor
OM	optical microscope
ORNL	Oak Ridge National Laboratory
PLS	proportional limit stress
PyC	pyrolytic carbon
SA3	Tyranno™ SA3
SCS	SCS-Ultra™
SEM	scanning electron microscope
SiC	silicon carbide
SiC/SiC	silicon carbide fiber-reinforced SiC matrix
STEM	scanning transmission electron microscopy
TEM	transmission electron microscopy
UFS	ultimate flexural strength

INTENTIONALLY BLANK

PIE OF NUCLEAR- GRADE SIC/SIC FLEXURAL COUPONS IRRADIATED TO 10 DPA AT LWR TEMPERATURE

INTRODUCTION

Silicon carbide (SiC)/SiC composites have historically been investigated for high-temperature structural applications in fusion and advanced fission energy systems. [1] Research and development (R&D) of SiC/SiC composites for various applications under different reactor operating conditions accumulated irradiation data for various temperature and dose conditions. The R&D finding was insignificant irradiation-induced degradation of the mechanical properties of nuclear-grade SiC/SiC composites consisting of high-crystalline SiC fibers and matrix at a temperature range of 300–1300°C and a low neutron dose (<~10 displacements per atom, or dpa). [2]

Recently, SiC/SiC composites have been examined for relatively low-temperature nuclear applications, including accident-tolerant fuel cladding and LWR channel boxes, [1, 3-5] because of their inherent high-temperature oxidation resistance [6] in addition to the irradiation resistance previously addressed. However, in fact, few researchers have investigated how irradiation at an LWR coolant temperature of ~300°C affects the composite's mechanical properties; and the maximum irradiation doses previously investigated were only up to ~3.4 dpa [7, 8]. Recently, Katoh et al. reported that irradiation at 300°C to ~70 dpa significantly degraded the strength of a specific nuclear-grade SiC/SiC composite—a chemical vapor infiltrated (CVI) SiC matrix composite with ~50 nm stacking of SiC/PyC (pyrolytic carbon) multilayer interphase coated HNS SiC fibers [9]. The degradation was attributed to both reduction in the fiber strength and degradation of the functionality of the multilayer interphase based on the flexural behavior and microstructures. [9] Note that this degradation at high dose was an issue for a low irradiation temperature. That CVI SiC/SiC composite showed only moderate mechanical degradation after irradiation at ~800°C to ~70 dpa. Although the study by Katoh et al. clearly showed degradation of the irradiated CVI SiC/SiC composites, the critical dose and the detailed mechanism of the degradation remain unclear.

The present study investigated the properties of SiC/SiC composites neutron irradiated at a near LWR-coolant-relevant temperature up to a dose exceeding the anticipated lifetime exposure for LWR fuel cladding. [10] The composites investigated were fabricated by the CVI method, a processing route for forming a high-purity SiC matrix. Since the HNS fiber composite reportedly degraded at a high dose of 70 dpa, this study investigated CVI SiC/SiC composites with SA3 and SCS SiC fibers in addition to HNS fibers. CVI SiC/SiC composites with HNS and SA3 fibers are currently being investigated as candidate LWR cladding materials. [4, 11, 12]

EXPERIMENTS

Three types of SiC/SiC composites were used for the irradiation study: (1) CVI SiC/SiC with 2-dimensional (2D) satin-weave HNS fiber reinforcement in a 0°/90° stacking configuration, (2) CVI SiC/SiC with 2D satin-weave SA3 fiber reinforcement in a 0°/90° stacking configuration, and (3) a 0/90º cross-ply laminated CVI SiC/SiC composite with SCS fiber. The fiber/matrix interphase was PyC for all the composites. The CVI process was conducted by Rolls-Royce High Temperature Composites Inc. (lot number: 13C-529). Key properties of those unirradiated SiC/SiC composites are summarized in Table 1.

The estimated fiber volume fraction and porosity were ~40% and 8–16 %, respectively; these values were similar to those of CVI SiC/SiC composites previously investigated, except that the SCS composite fiber had less porosity. [2]

The HNS and SA3 fibers are classified among near-stoichiometric SiC fibers consisting of high-crystalline β-SiC and a free carbon phase, as reported by the vendor. The nominal fiber diameter is 12 μm for HNS and 7.5 μm for SA3. The major difference in their microstructures is grain size: ~50 nm for HNS and ~200 nm for SA3. SCS is a different class of SiC fiber consisting of a chemically vapor deposited (CVD) SiC phase on a carbon core. The nominal fiber diameter is ~140 μm. The CVD SiC phase near both the carbon core and outer surface was reported to be carbon-rich SiC. [13]

The SiC/SiC plates were machined to bar specimens with dimensions of 25×2.8×1 mm^3 for the irradiation experiment. The fiber reinforcements were parallel to the specimen length and width directions. Neutron irradiation was conducted at the High Flux Isotope Reactor at Oak Ridge National Laboratory. The neutron dose was 2.0×10^{25} and 11.8×10^{25} n/m^2 (E >0.1 MeV), equivalent to 2.0 and 11.8 dpa, respectively, assuming that 1×10^{25} n/m^2 (E>0.1 MeV) corresponds to 1 dpa. [14] Details of the irradiation capsule design and calculated temperature distribution within the specimens during irradiation are reported in Appendix A. The irradiation temperature was 230–340°C, which was experimentally determined based on the recovery behavior of a passive SiC thermometer made of high-purity CVD SiC (Dow Chemical Co., Marlborough, Massachusetts) during dilatometry [15]. Note that the specimens were designed to be irradiated in contact with the thermometer.

Table 1. Summary of unirradiated material properties

	Hi-Nicalon Type S CVI SiC/SiC composite	Tyranno SA3 CVI SiC/SiC composite	SCS-Ultra CVI SiC/SiC composite
Fiber type	Hi-Nicalon Type S	Tyranno SA3	SCS Ultra
Fiber architecture	2D satin-weave, 0°/90° stacking	2D satin-weave, 0°/90° stacking	0°/90° cross-ply laminate
Interphase	80–110 nm thick PyC	250–350 nm thick PyC	500–700 nm thick PyC
Matrix	CVI SiC	CVI SiC	CVI SiC
Estimated fiber volume fraction	~37%	~45%	~43%
Estimated porosity	~13%	~16%	~8%
Mass density	~2.70 g/cm^3	~2.61 g/cm^3	~2.85 g/cm^3

The mechanical properties and microstructures of the composites were evaluated before and after irradiation. The number of test specimens was 16–20 for the pre-irradiation experiments and 6–7 for post-irradiation experiments for each type of composite. The dynamic Young's moduli of the SiC/SiC composites were determined using the impulse excitation of vibration method in accordance with ASTM standard C1259–15, [16] using an Integrated Material Control Engineering resonant frequency and damping analyzer. Four point flexural tests using 4-point-1/4 point fixture with an outer span of 20 mm were conducted according to the general guidelines of ASTM C1341–13, [17] with the exception that the

narrower specimen width compared with the fiber weave unit cell of the HNS and SA3 composites was used in this study due to limitation of the specimen volume for irradiation vehicle. The proportional limit stress (PLS) was determined as a 5% deviation in stress from the initial linearity. All tests were conducted at ambient temperature. The dimensions of each specimen were obtained using a micrometer with a precision of <1μm, which measured length swelling at an accuracy of <0.08%. The surface morphology of the specimens was investigated using a KEYENCE VHX-1000 optical microscope. The fracture surfaces and polished cross sections of the composites were characterized using a Hitachi 4800S scanning electron microscope (SEM) for unirradiated specimens and an FEI Quanta Dual Beam SEM/focused ion beam (FIB) and an FEI Versa Dual Beam SEM/FIB for irradiated specimens. Transmission electron microscopy (TEM) observation was also conducted using a JEOL JEM2100F operated at 200 kV. The observation was conducted in scanning TEM (STEM) mode. The TEM specimens were prepared using the FEI Versa Dual Beam SEM/FIB operated at 30 kV for rough milling and 2 and 5 kV for final thinning, followed by low-energy ion milling using a Fischione Model 1040 NanoMill operated at 600 and 900 eV.

RESULTS

Fig. **1**a–c presents representative stress-strain curves during the flexural tests on unirradiated and irradiated specimens. Results of the analysis of flexural behavior are summarized in Fig. 1d–f and Table **2**. Regardless of irradiation, the HNS CVI SiC/SiC composites exhibited quasi-ductile fracture behavior: initial elastic behavior and then gradual modulus reduction up to the ultimate flexural strength (UFS), followed by progressive breaking. The limited effects of irradiation on PLS and UFS were identified for the HNS composites. For the SA3 CVI SiC/SiC composite specimens, the fracture behavior was also typical for the tough composites before and after irradiation. Although part of the specimens exhibited a sudden fracture after UFS, this phenomenon was found both with and without irradiation. For the SCS SiC/SiC composite specimens, analysis of the flexural behavior highlighted significant irradiation effects on the mechanical properties: the average UFS was degraded by 68% following irradiation to 11.8 dpa. In addition, the quasi-ductile, unirradiated materials became brittle following irradiation. On the other hand, the degradation of the PLS was apparent, considering the standard deviations.

For all three types of SiC/SiC composites, the dynamic Young's modulus tended to drop as a result of irradiation. The modulus reduction of the SCS composites by up to ~20% was the most significant result in this study. A higher dynamic Young's modulus than the tangent modulus of elasticity from the flexural tests was obtained in this study, which was also reported in the previous work [9]. The length swelling of the three types of composites ranged between 0.59 and 0.75% and was dose-insensitive. It is important to note that this result was similar to or less than the swelling of the CVD SiC thermometer (~0.7%) irradiated along with the composites.

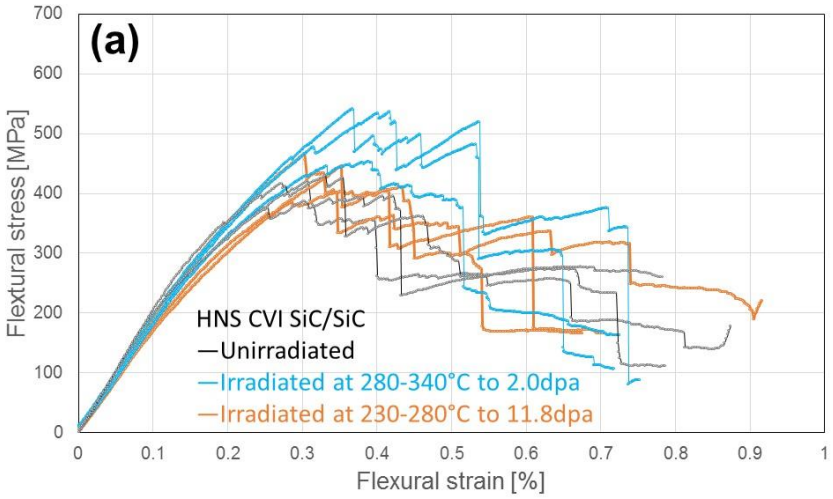
(a)
HNS CVI SiC/SiC
—Unirradiated
—Irradiated at 280-340°C to 2.0dpa
—Irradiated at 230-280°C to 11.8dpa
Flextural stress [MPa]
Flexural strain [%]

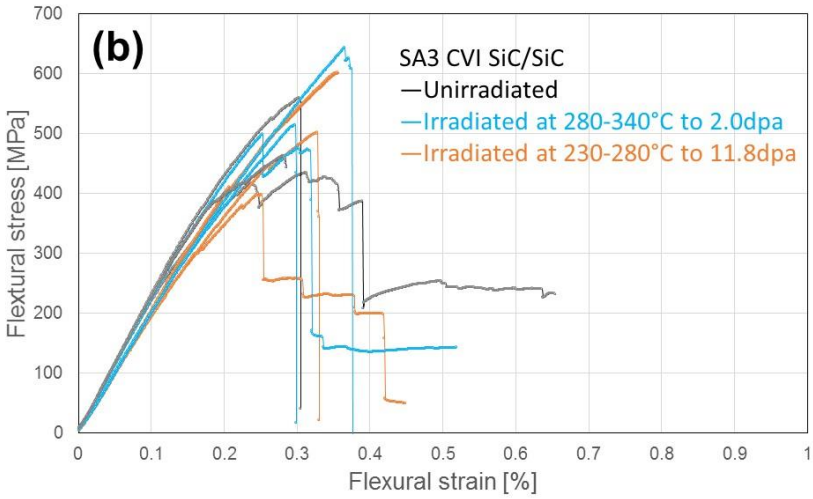
(b)
SA3 CVI SiC/SiC
—Unirradiated
—Irradiated at 280-340°C to 2.0dpa
—Irradiated at 230-280°C to 11.8dpa
Flextural stress [MPa]
Flexural strain [%]

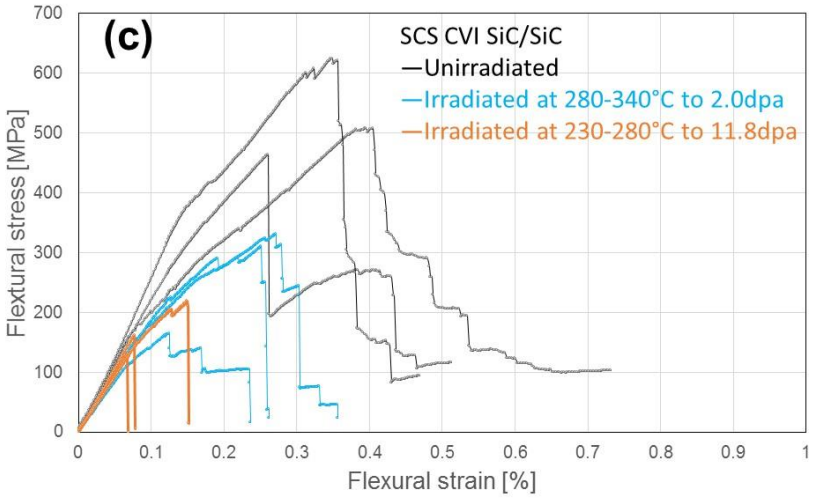
(c)
SCS CVI SiC/SiC
—Unirradiated
—Irradiated at 280-340°C to 2.0dpa
—Irradiated at 230-280°C to 11.8dpa
Flextural stress [MPa]
Flexural strain [%]

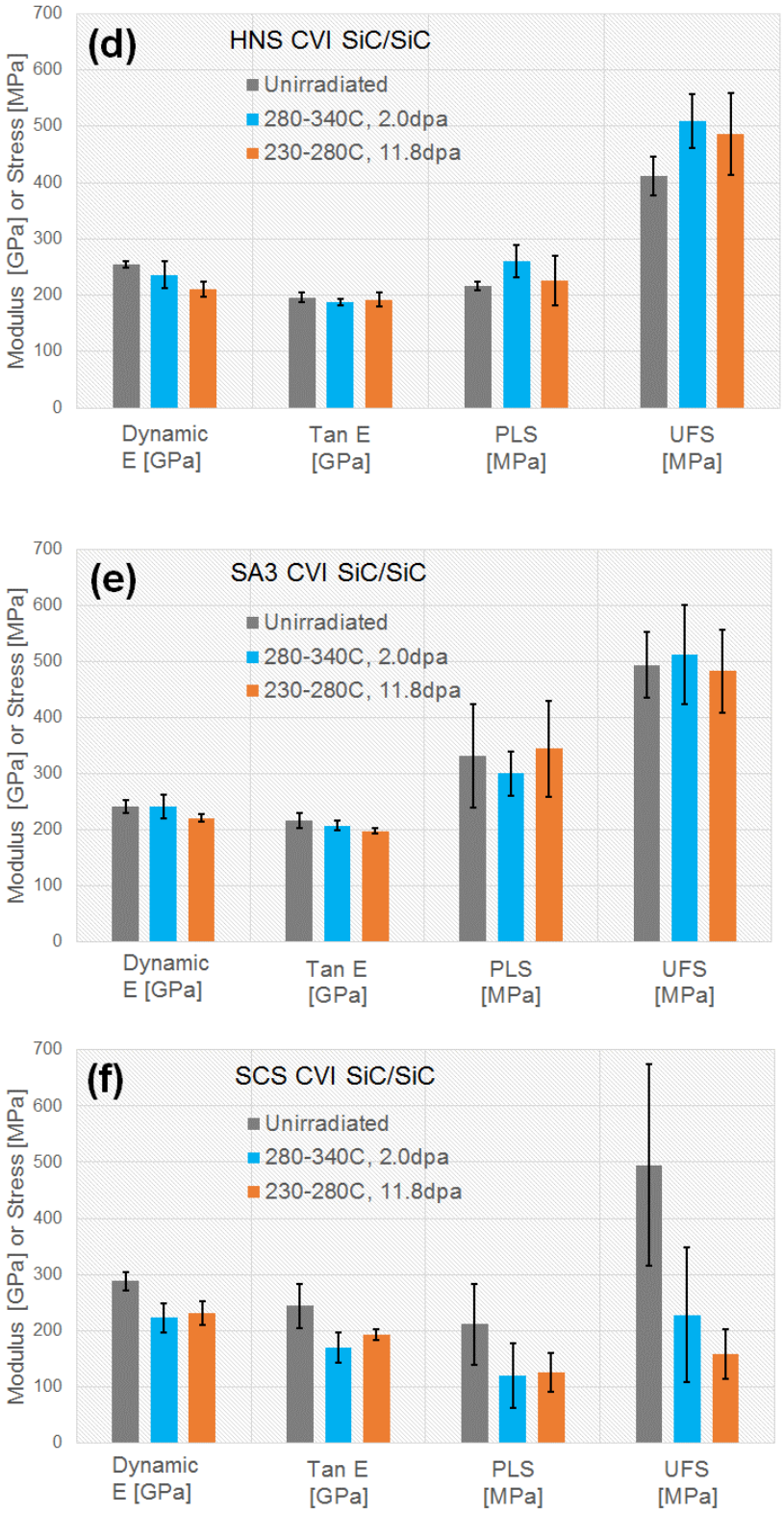

Fig. 1. Representative flexural behavior of unirradiated and irradiated SiC/SiC composites with (a) HNS, (b) SA3, and (c) SCS fibers, and summary of the mechanical properties (d–f). Note that complete fracture could not be achieved for failure strain beyond ~0.7 % because of contact between specimen and fixture. Dynamic E and Tan E stand for dynamic Young's modulus and tangent modulus of elasticity, respectively.

Table 2. Mechanical properties and swelling of unirradiated and irradiated CVI SiC/SiC composites with three different SiC fibers. Parentheses indicate the one standard deviation.

Material	Irradiation conditions	Dynamic Young's modulus (GPa)	Tangent modulus of elasticity (GPa)	PLS (MPa)	UFS (MPa)	Length swelling (%)	Number of tests
HNS CVI SiC/SiC	Unirradiated	255 (6)	196 (8)	216 (8)	412 (35)	0	20
	280–340°C/2.0dpa	236 (24)	187 (5)	260 (28)	509 (49)	0.68 (0.06)	6
	230–280°C/11.8dpa	210 (13)	192 (13)	226 (45)	486 (72)	0.70 (0.03)	6
SA3 CVI SiC/SiC	Unirradiated	241 (11)	216 (14)	331 (91)	493 (59)	0	20
	280–340°C/2.0dpa	241 (22)	207 (8)	300 (40)	513 (87)	0.65 (0.05)	7
	230–280°C/11.8dpa	220 (7)	198 (4)	344 (85)	482 (74)	0.59 (0.03)	7
SCS CVI SiC/SiC	Unirradiated	288 (17)	243 (40)	211 (72)	495 (178)	0	16
	280–340°C/2.0dpa	223 (25)	170 (27)	120 (57)	228 (121)	0.71 (0.03)	7
	230–280°C/11.8dpa	230 (21)	193 (9)	126 (34)	159 (44)	0.75 (0.06)	6

Fracture surfaces of the flexural tested specimens were observed using SEM, as shown in Fig. 2. The observations of the irradiation specimens were conducted for only the higher-dose condition. Both unirradiated and irradiated HNS SiC/SiC composites exhibited long (up to ~700 μm) fiber pullout (Fig. **2**a, b). Shorter fiber pullout was also observed at the higher magnification. These observations indicate effective deflection of matrix cracks during breaking and were consistent with the flexural behavior of the tough composites. Rough fracture surfaces of the unirradiated and irradiated HNS fibers were observed. In summary, no notable change in the fracture appearance resulting from irradiation was found in the HNS SiC/SiC composites. There is satisfactory agreement between the stabilities of the mechanical properties and the microstructure.

For the SA3 SiC/SiC composite, also, the effect of irradiation on the fracture behavior was not obvious. Both unirradiated and irradiated composites typically showed ~100 μm relatively short fiber pullout (Fig. **2**c, d), and the long fiber pullout observed in the HNS SiC/SiC composites was not common in this composite. The lower degree of fiber pullout explains the relatively limited failure strain of the SA3 composite compared with the HNS composite. No noteworthy difference was found between the fiber fracture surfaces before and after irradiation. Again, the microstructural stability was consistent with the flexural behavior of this composite.

As expected based on the flexural behavior, irradiation significantly affected the fracture appearance of the SCS SiC/SiC composite. The unirradiated composite showed fiber/matrix delamination, which is a toughening mechanism of this composite (Fig. 2e). On the other hand, a flat fracture surface without delamination and only ~50 μm fiber pullout were observed following irradiation (Fig. 2f), which is in good agreement with brittle fracturing following irradiation.

Polished cross sections of the SiC/SiC specimens not subjected to flexural testing were also observed before and after irradiation, as shown in Fig. 3. The SEM observation found that the PyC interphase with ~100 nm thickness in the unirradiated HNS SiC/SiC composites was preserved following irradiation. This observation could not evaluate the microstructural change in the HNS fiber because of the small grain size (~50 nm). The unirradiated SA3 SiC/SiC composite possessed a relatively thicker PyC interphase with a 250–350 nm thickness. The interphase thickness appeared not to be changed by irradiation. The microstructural stability of the PyC interphase is reasonable considering the quasi-ductile fracture behavior before and after irradiation. In the SA3 fiber, a carbon impurity phase was found in the backscattered electron micrographs with a black contrast. The carbon phase was more concentrated near the center of the fiber, as observed in both unirradiated and irradiated SA3 fibers. The PyC interphase in the SCS SiC/SiC composites was also preserved following irradiation. However, irradiation-induced

cracking occurred within the fiber. The cracks appeared to initiate from the outer surface of the carbon core and proceed to the CVD SiC phase in the fiber. This cracking within the CVD SiC phase was frequently observed in each fiber cross section in the irradiated specimens, but it was never found in the unirradiated specimens. The cracking is evidence of degradation of the fiber strength.

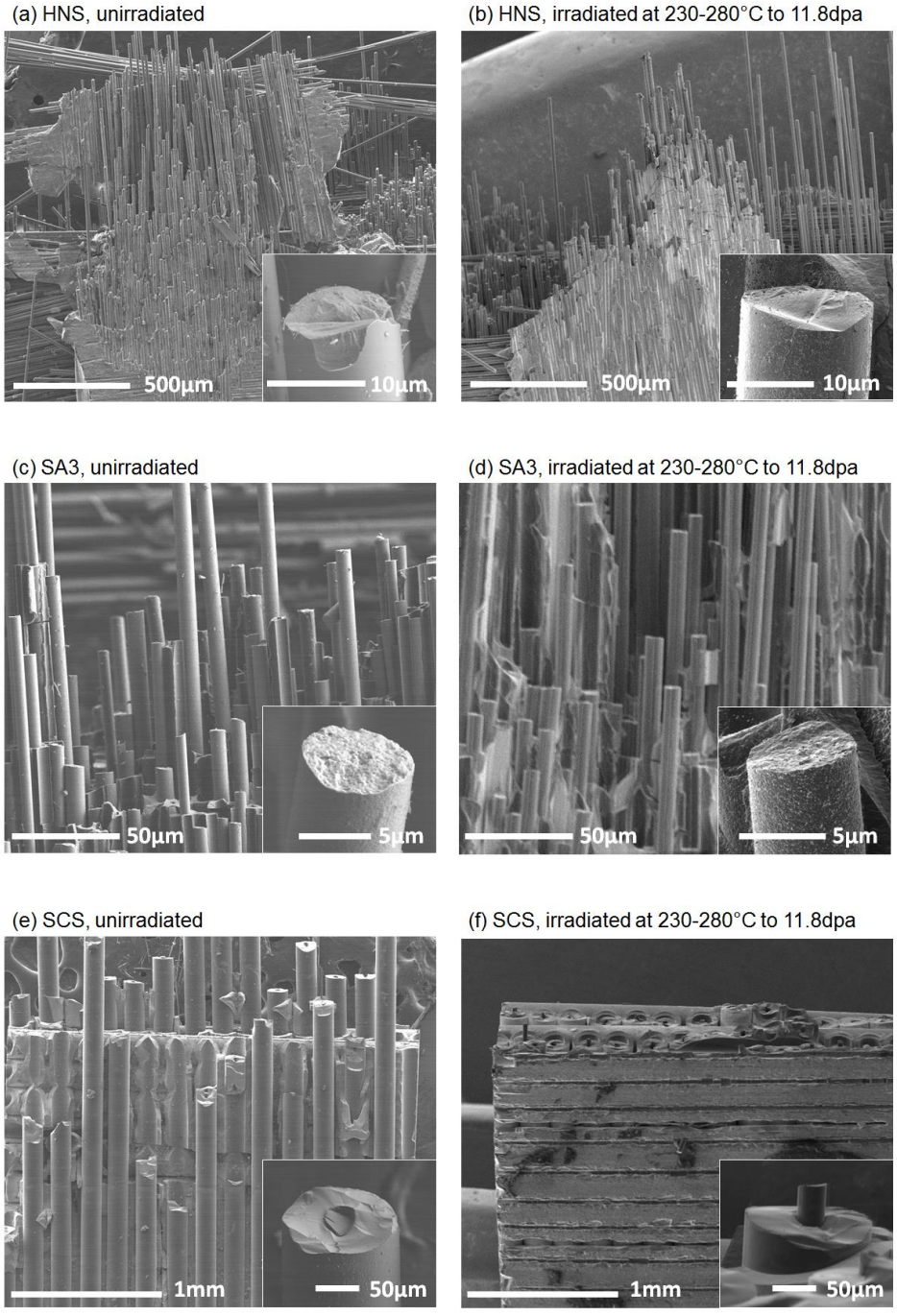

Fig. 2. Secondary electron images of fracture surfaces of SiC/SiC composites unirradiated and irradiated to 230–280°C to 11.8dpa: (a) unirradiated HNS, (b) irradiated HNS, (c) unirradiated SA3, (d) irradiated SA3, (e) unirradiated SCS, and (f) irradiated SCS SiC/SiC composites. Inserted images show the fiber fracture surfaces.

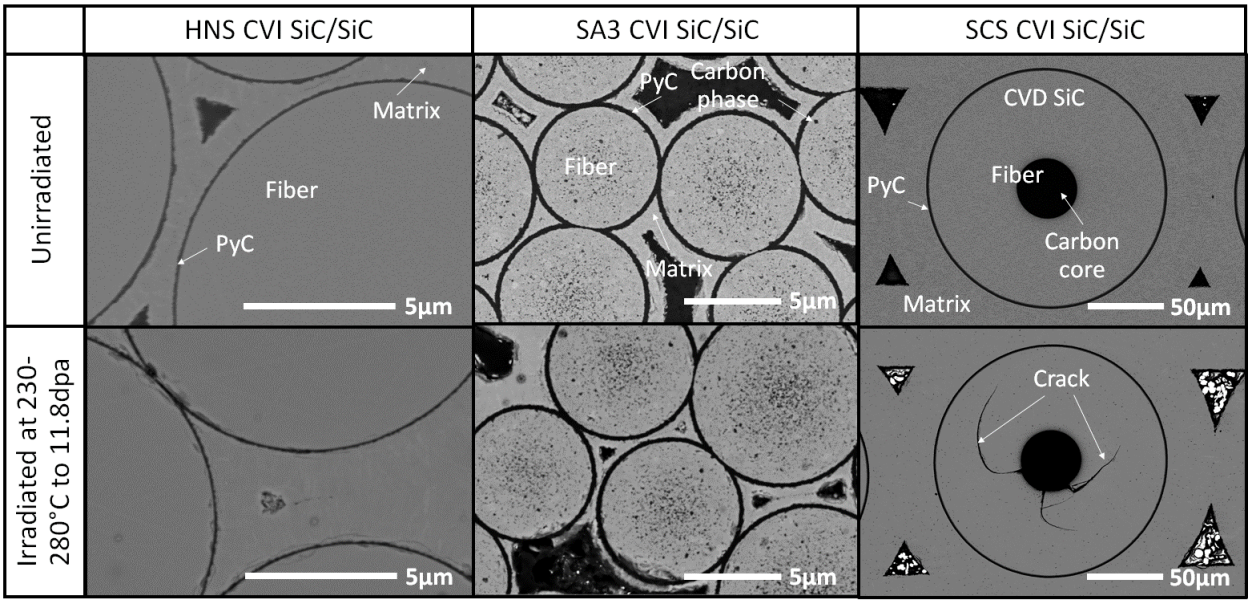

Fig. 3. Backscattered electron micrographs of HNS, SA3, and SCS CVI SiC/SiC composites with and without irradiation at 230–280°C to 11.8dpa.

The microstructural stability of the HNS fibers was investigated by STEM. Fig. 4 shows STEM bright field (BF), high-angle annular dark field (HAADF), and processed HAADF images taken from the near centers of the HNS fibers unirradiated and irradiated at 230–280°C to 11.8dpa. The pair of BF and HAADF images were taken from the same location. The black and white contrast in the BF images indicate the SiC grain and carbon phase, respectively, and the contrast is vice versa in the HAADF image. The SiC grain size was typically less than 50 nm. The HAADF images were processed to produce a binary image for analysis of the size distribution of the carbon secondary phase, as shown in Fig. 4c and f. All the images analyzed were taken from an area with a 60–70 nm foil thickness evaluated by a log-ratio method via electron energy loss spectroscopy. In addition, the same imaging condition, image processing, and manner of analysis were applied to the micrographs from the unirradiated and irradiated specimens. The analysis results shown in Fig. 5 are evidence that the size distribution and number density of the carbon phase were similar in the unirradiated and irradiated materials.

Fig. **6**a shows untreated bend bar specimen surfaces of the SCS SiC/SiC composites unirradiated and irradiated at 280–280°C to 11.8dpa; they were obtained using optical microscopy (OM). The observation found cracking of the irradiated carbon core, which was absent on the unirradiated surfaces. An irradiated carbon core with substantial cracks is considered not to contribute to the fiber strength. Another observation using focus variation OM evaluated the surface topology (Fig. 6b). Although the unirradiated surface was relatively flat, the irradiated surface exhibited a dip at the carbon core. The step between the carbon core and the CVD SiC region was ~20 µm, which corresponds to at least ~0.7% shrinkage of the fiber along the fiber axis, considering the ~0.7% swelling of SiC. There is no indication of significant differential swelling between the SiC matrix and the CVD SiC fiber region, based on the topologic OM analysis.

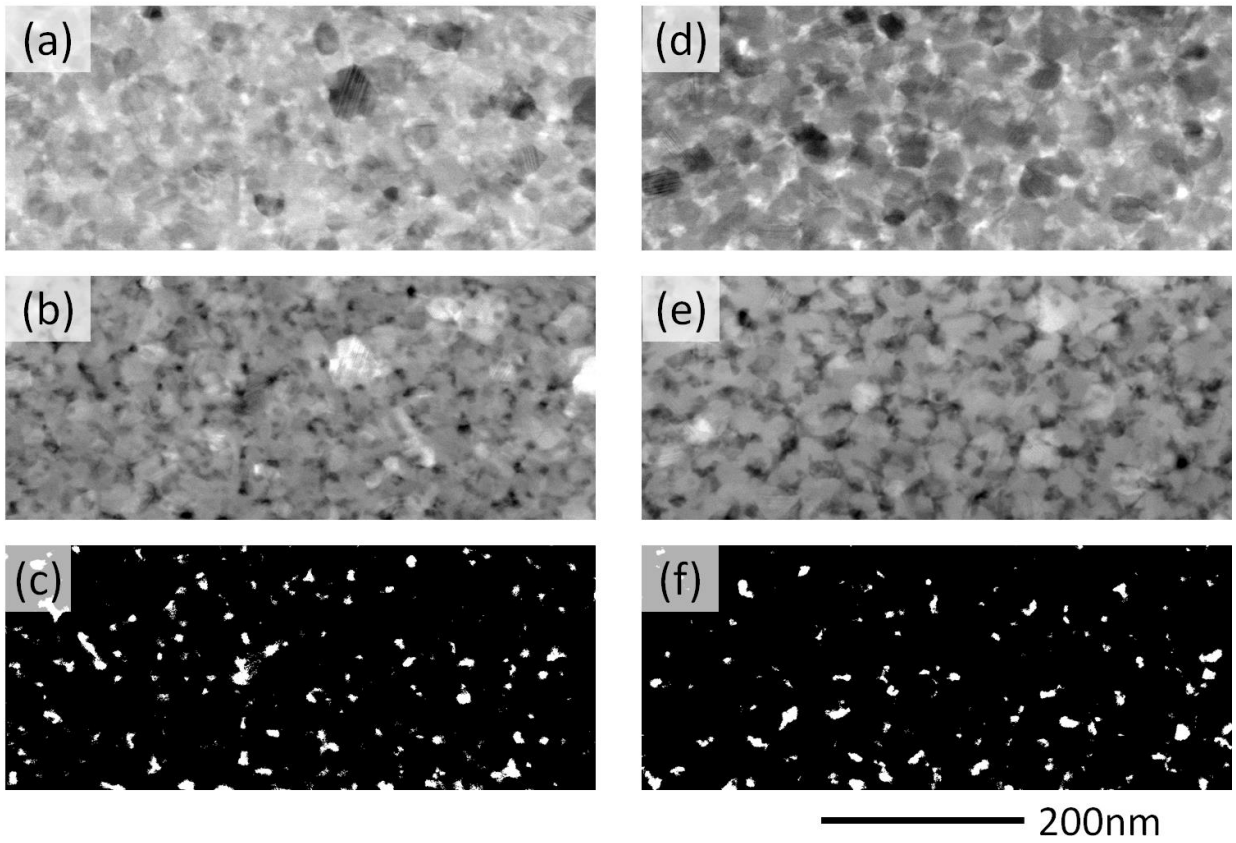

Fig. 4. STEM micrograph of HNS fibers: (a) BF, (b) HAADF, and (c) processed HAADF images of the unirradiated fibers; (d) BF, (e) HAADF, and (f) processed HAADF images of the fibers irradiated at 230–280°C to 11.8dpa. The sets of BF, HAADF, and processed HAADF images were taken from the same location. The foil thicknesses of both the unirradiated and irradiated materials ranged from 60 to 70 nm.

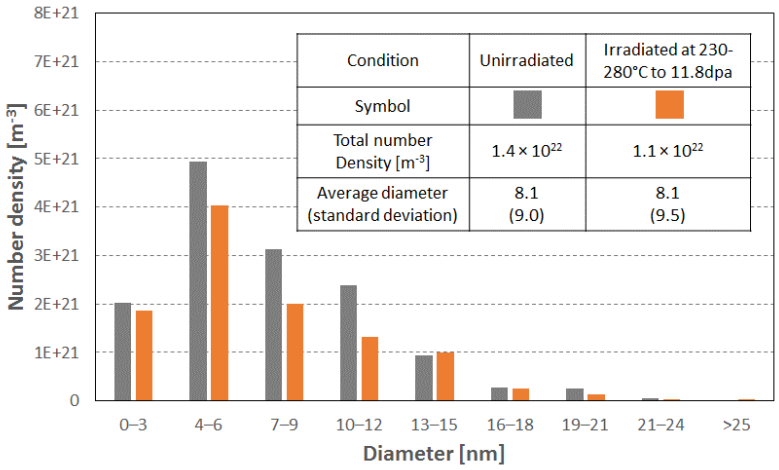

Fig. 5. Result summary of TEM image analysis of the size distribution of the secondary phase in unirradiated and irradiated HNS fibers. The diameter of a circle of an equal projection area is used to define the size of the secondary phase.

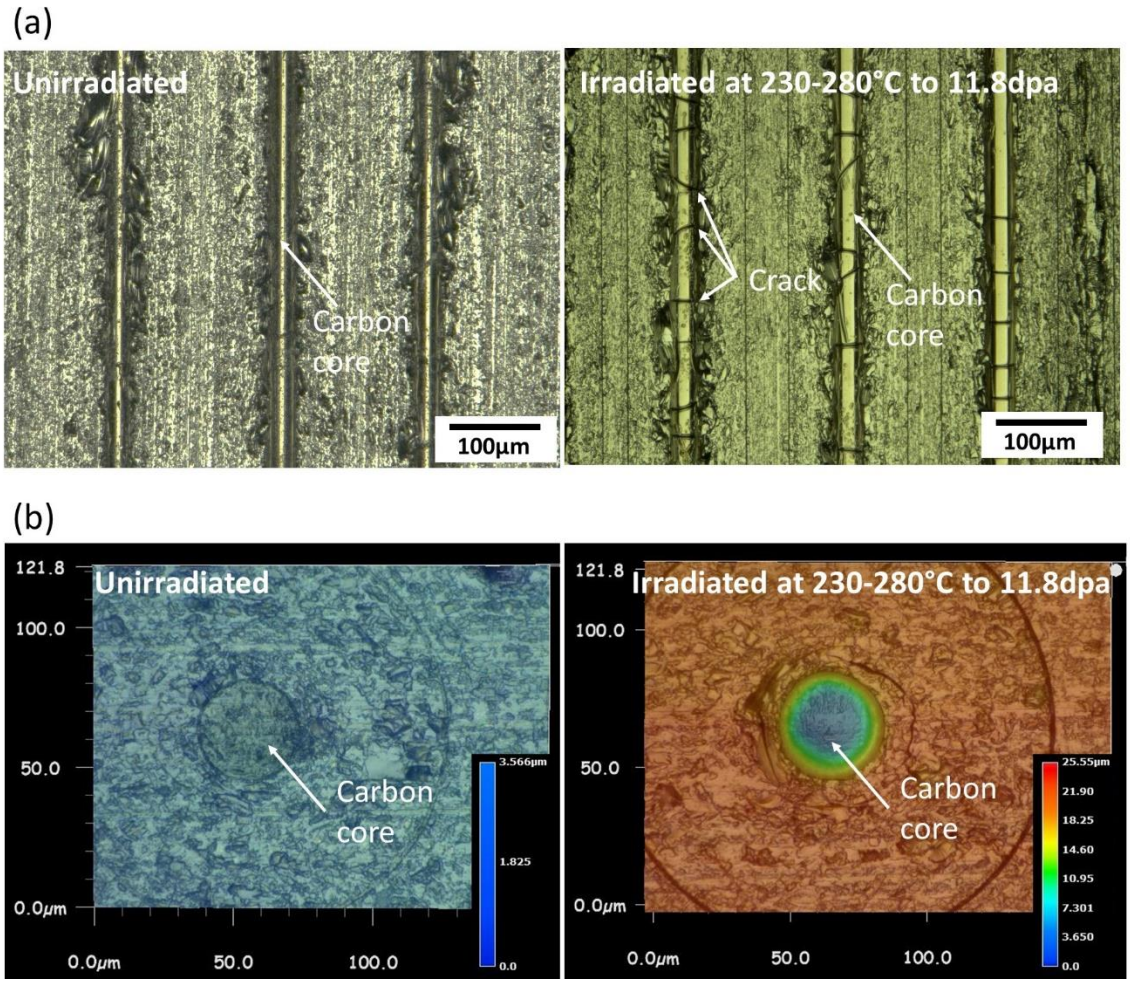

Fig. 6. Optical microscopy (OM) images compared between reference and as-irradiated surfaces of SCS CVI SiC/SiC composite: (a) conventional OM image, and (b) layered image of OM and topographic images. The topographic information was obtained via focus variation OM. The fiber axis was parallel to the specimen length and width directions in images (a) and (b), respectively.

DISCUSSION

This study found that the HNS and SA3 SiC/SiC composites retained their PLS and UFS and did not undergo a significant reduction in Young's modulus (less than 18%) following irradiation at ~300°C up to 11.8 dpa. In addition, there was no progressive swelling from 2.0 to 11.8 dpa. Since previous irradiation studies achieved only ~3 dpa at such a low temperature, [7, 8] this higher-dose irradiation study demonstrated more encouraging results for the development of SiC-based LWR core structures. The irradiation-resistant mechanical properties of the HNS and SA3 SiC/SiC composites are understandable, since there were no obvious irradiation-induced changes in fiber pullout length, fiber fracture surface, interphase appearance, or fiber microstructure. The reduction of the Young's moduli was considered a result of the lattice expansion of the SiC phases. [7, 18] It is worth highlighting that this study provided positive results for the irradiation resistance of HNS and SA3 CVI SiC/SiC composites, which are widely being considered as SiC-based materials for fuel cladding applications. [3-5]

In previous high-dose irradiation studies up to 70 dpa, it was reported that the strength reduction of the irradiated HNS fiber was accompanied by a smooth fiber fracture surface and modification of the carbon phase distribution in the fibers. [9, 19]. The present study supports the idea that those features, which were absent in the irradiation-resistant HNS composites in this study, are keys to understanding the degradation mechanism. In the case of the SA3 CVI SiC/SiC composites, there has been no report of significant strength reduction of the irradiated fiber following irradiation up to ~10 dpa [7], and a higher neutron irradiation study has not been reported.

Regarding the SCS SiC/SiC composites, the degradation of UFS and brittle fracture behavior following irradiation discourages the use of this material in the irradiation environments investigated. Given that the matrix of high-purity CVI SiC was proved to be radiation tolerant, [18] the material degradation is suspected to be caused by changes in the mechanical properties of the fiber and/or the interfacial properties of the fiber/matrix interface. Fiber degradation was evidenced by the irradiation-induced cracking in the carbon core (Fig. 6) and the CVD SiC phase in the fibers (Fig. 3). The ultimate strength of SiC/SiC composites under a uniaxial tensile stressed condition is governed by the fiber statistical strength, in theory, with an assumption of an effective deflection of matrix cracking at the interface. [20] It is thought that the fiber strength contributed to the UFS, since short fiber pullout was observed, as shown in Fig. 2f. Regarding the interfacial properties of the PyC, a key function is an ability to cause fiber/matrix debonding to deflect matrix cracking. The resultant fiber bridging followed by fiber pullout with interfacial dissipation is a mechanism of nonlinear fracture behavior of the SiC/SiC composites. [21] The crack deflection or propagation at the interface depends on the constituent strength and the Young's moduli, based on the Cook and Gordon mechanism. This mechanism suggests that fiber degradation potentially contributes to crack propagation, i.e. brittle fracture. [22] Although the degradation of the interface properties was not quantified by an experiment in this study, the cracking of the SCS fibers is a critical issue for the SCS composite.

The cracking mechanism can be explained by the differential swelling between the carbon core and the surrounding CVD SiC phase. The lesser swelling in the carbon core than in the SiC phase along the fiber axial direction, confirmed by focus variation OM (Fig. 6b), resulted in an axial tensile residual stress within the carbon core, which consequently caused cracking of the carbon core vertical to the fiber axis (Fig. 6a). This is consistent with the swelling behavior of glassy carbon, a material of the carbon core. This type of material tends to shrink under exposure to neutron irradiation at a wide range of temperatures (90–750°C),[23] whereas SiC swells. [18] The cracking of the CVD SiC phase starting from the outer surface of the carbon core (Fig. 3) may also be a result of the differential swelling. The carbon core is expected to swell more than the CVD SiC along fiber radius direction in contrast to the fiber axial direction. Although the comparison of the radial swelling could not be conducted by the experiment of this study, previous study indicated that diametric swelling and axial shrinkage of an irradiated carbon fiber based on the anisotropic swelling of a carbon fiber composite dependent on the fiber architecture [24]. Therefore, the discussion on the cracking mechanism is consistent with the previous studies. In summary, the anisotropic swelling of the carbon core and the differential swelling can explain the irradiation-induced cracking. A solution minimizing that differential swelling is reduction of the carbon core volume, which is expected to improve irradiation resistance of the SCS SiC/SiC composites.

The HNS, SA3, and SCS fibers all contained a carbon secondary phase within the material, but the differential swelling between the two phases caused cracking only in the SCS fiber. Note that the differential swelling occurred in all three fibers, since the SiC and the carbon phases do not swell in exactly the same manner. The impact of the differential swelling is expected to depend on the phase fraction, distribution, and swelling behaviors of the phases. The results from this study imply that finely distributed carbon phases (HNS and SA3), rather than separated phases (SCS), have advantages to mitigate the strain from the differential swelling. This mechanism could operate in the HNS and SA3

fibers by effective irradiation creep in the SiC and/or carbon phases with a substantial interface. Another implication is that the magnitude of the differential swelling between the carbon phase and the SiC phase in the HNS and SA3 fibers was relatively smaller than in the SCS fiber. This implication is based on the swelling behavior of the carbon materials, which is highly dependent on material qualities such as density and material anisotropy, [24, 25] though Values for the swelling of the carbon phases in the HNS and SA3 fibers are not currently available.

Since the irradiation resistance of the HNS and SA3 SiC/SiC composites was proven at ~300°C up to 11.8 dpa in this study, an area of future work for the development of SiC-based LWR core structures will be a higher-dose irradiation study to investigate the lifetime dose for these composites. Future work also should involve determination of the synergy between irradiation effects and other environmental effects, such as hydrothermal corrosion. These areas have been the subjects of limited investigation [26, 27], but they are considered a critical and important feasibility issue.

CONCLUSIONS

This study proved the excellent resistance of HNS and SA3 CVI SiC/SiC composites to neutron irradiation at near–LWR-coolant temperatures of 230–340°C to doses of 2.0 and 11.8dpa. There was no obvious change in the flexural strength (PLS or UFS) by irradiation. The irradiated composites retained their quasi-ductile fracture behavior. It was confirmed that the swelling saturates below 2.0 dpa. The microstructural observations supported the irradiation resistance of the mechanical properties: there was no notable irradiation effect on the fiber pullout behavior, fiber fracture surface, and interphase thickness. These results confirm that HNS and SA3 CVI SiC/SiC composites are appropriate for use as LWR fuel cladding and core structural materials in terms of their tolerance to neutron irradiation.

In contrast, significant mechanical degradation was found in SCS fiber-reinforced CVI SiC/SiC composites following irradiation. Neutron irradiation to 11.8 dpa caused the transition of the fracture mode from quasi-ductile to brittle, accompanying a 68% decrease in the UFS. The microstructural analysis identified irradiation-induced cracking within the SCS fibers as the primary reason for the degradation. The cracking was likely caused by the differential swelling between the carbon fiber core and the surrounding CVD SiC phase. Thus, CVD SiC fibers with carbon fiber cores are not suitable for use in nuclear applications.

REFERENCES

[1] Y. Katoh, L.L. Snead, C.H. Henager, T. Nozawa, T. Hinoki, A. Iveković, S. Novak, S.G. de Vicente, Current status and recent research achievements in SiC/SiC composites, Journal of Nuclear Materials 455(1) (2014) 387-397.
[2] Y. Katoh, K. Ozawa, C. Shih, T. Nozawa, R.J. Shinavski, A. Hasegawa, L.L. Snead, Continuous SiC fiber, CVI SiC matrix composites for nuclear applications: Properties and irradiation effects, Journal of Nuclear Materials 448(1) (2014) 448-476.
[3] E. Rohmer, E. Martin, C. Lorrette, Mechanical properties of SiC/SiC braided tubes for fuel cladding, Journal of Nuclear Materials 453(1) (2014) 16-21.
[4] D. Kim, H.-G. Lee, J.Y. Park, W.-J. Kim, Fabrication and measurement of hoop strength of SiC triplex tube for nuclear fuel cladding applications, Journal of Nuclear Materials 458 (2015) 29-36.
[5] C. Deck, G. Jacobsen, J. Sheeder, O. Gutierrez, J. Zhang, J. Stone, H. Khalifa, C. Back, Characterization of SiC–SiC composites for accident tolerant fuel cladding, Journal of Nuclear Materials 466 (2015) 667-681.
[6] K.A. Terrani, B.A. Pint, C.M. Parish, C.M. Silva, L.L. Snead, Y. Katoh, Silicon carbide oxidation in steam up to 2 MPa, Journal of the American Ceramic Society 97(8) (2014) 2331-2352.
[7] Y. Katoh, L.L. Snead, T. Nozawa, S. Kondo, J.T. Busby, Thermophysical and mechanical properties of near-stoichiometric fiber CVI SiC/SiC composites after neutron irradiation at elevated temperatures, Journal of Nuclear Materials 403(1) (2010) 48-61.
[8] G. Newsome, L.L. Snead, T. Hinoki, Y. Katoh, D. Peters, Evaluation of neutron irradiated silicon carbide and silicon carbide composites, Journal of Nuclear Materials 371(1) (2007) 76-89.
[9] Y. Katoh, T. Nozawa, C. Shih, K. Ozawa, T. Koyanagi, W. Porter, L.L. Snead, High-dose neutron irradiation of Hi-Nicalon Type S silicon carbide composites. Part 2: Mechanical and physical properties, Journal of Nuclear Materials 462 (2015) 450-457.
[10] S.J. Zinkle, G. Was, Materials challenges in nuclear energy, Acta Materialia 61(3) (2013) 735-758.
[11] F. Bernachy-Barbe, L. Gélébart, M. Bornert, J. Crépin, C. Sauder, Anisotropic damage behavior of SiC/SiC composite tubes: Multiaxial testing and damage characterization, Composites Part A: Applied Science and Manufacturing 76 (2015) 281-288.
[12] C. Deck, H. Khalifa, B. Sammuli, T. Hilsabeck, C. Back, Fabrication of SiC–SiC composites for fuel cladding in advanced reactor designs, Progress in Nuclear Energy 57 (2012) 38-45.
[13] H. Yugami, S. Nakashima, A. Mitsuishi, A. Uemoto, M. Shigeta, K. Furukawa, A. Suzuki, S. Nakajima, Characterization of the free-carrier concentrations in doped β-SiC crystals by Raman scattering, Journal of applied physics 61(1) (1987) 354-358.
[14] H.L. Heinisch, L.R. Greenwood, W.J. Weber, R.E. Williford, Displacement damage in silicon carbide irradiated in fission reactors, Journal of nuclear materials 327(2) (2004) 175-181.
[15] A.A. Campbell, W.D. Porter, Y. Katoh, L.L. Snead, Method for analyzing passive silicon carbide thermometry with a continuous dilatometer to determine irradiation temperature, Nuclear Instruments and Methods in Physics Research Section B: Beam Interactions with Materials and Atoms 370 (2016) 49-58.
[16] ASTM C1259-15: Standard test method for dynamic Young's modulus, shear modulus, and Poisson's ratio for advanced ceramics by impulse excitation of vibration, (2015).
[17] ASTM C1341-13: Standard Test Method for Flexural Properties of Continuous Fiber-Reinforced Advanced Ceramic Composites, (2013).
[18] L.L. Snead, T. Nozawa, Y. Katoh, T.-S. Byun, S. Kondo, D.A. Petti, Handbook of SiC properties for fuel performance modeling, Journal of nuclear materials 371(1) (2007) 329-377.
[19] A.G. Perez-Bergquist, T. Nozawa, C. Shih, K.J. Leonard, L.L. Snead, Y. Katoh, High dose neutron irradiation of Hi-Nicalon Type S silicon carbide composites, Part 1: Microstructural evaluations, Journal of Nuclear Materials 462 (2015) 443-449.
[20] W.A. Curtin, Theory of Mechanical Properties of Ceramic-Matrix Composites, Journal of the American Ceramic Society 74(11) (1991) 2837-2845.

[21] A. Evans, F. Zok, The physics and mechanics of fibre-reinforced brittle matrix composites, Journal of Materials Science 29(15) (1994) 3857-3896.
[22] S. Pompidou, J. Lamon, Analysis of crack deviation in ceramic matrix composites and multilayers based on the Cook and Gordon mechanism, Composites science and technology 67(10) (2007) 2052-2060.
[23] Y.S. Virgil'ev, I. Lebedev, Effect of neutron irradiation on properties of glassy carbon, Inorganic materials 38(7) (2002) 668-673.
[24] L. Snead, T. Burchell, Y. Katoh, Swelling of nuclear graphite and high quality carbon fiber composite under very high irradiation temperature, Journal of Nuclear Materials 381(1) (2008) 55-61.
[25] J. Kaae, The mechanical behavior of BISO-coated fuel particles during irradiation. Part I: Analysis of stresses and strains generated in the coating of a BISO fuel particle during irradiation, Nuclear Technology 35(2) (1977) 359-367.
[26] S. Kondo, M. Lee, T. Hinoki, Y. Hyodo, F. Kano, Effect of irradiation damage on hydrothermal corrosion of SiC, Journal of Nuclear Materials 464 (2015) 36-42.
[27] J.D. Stempien, D.M. Carpenter, G. Kohse, M.S. Kazimi, Characteristics of composite silicon carbide fuel cladding after irradiation under simulated PWR conditions, Nuclear Technology 183(1) (2013) 13-29.

Appendix A

Design of Irradiation Vehicle and Simulation of Temperature of Specimens during Irradiation

A schematic image of a capsule housing configuration is shown in Fig. A1. The specimen holders were made of V-4Cr-4Ti alloy. Each capsule contained 20 composite bar specimens (6 HNS, 7 SA3, and 7 SCS) and four monolithic CVD SiC passive thermometers. Additional CVD SiC materials were located between the SiC/SiC specimens and the holder to prevent any contamination of the specimens from the metallic holder during the irradiation. Springs made of CVD SiC were also used to maintain physical contact between the holder and the internal SiC materials to control the irradiation temperature.

Irradiation capsules were designed to control specimen temperatures using 3-dimensional thermal analysis with ANSYS software. Figure A2 shows the simulation results. The expected temperature gradients in the SiC/SiC and CVD SiC specimens were within 10% of the average specimen temperatures.

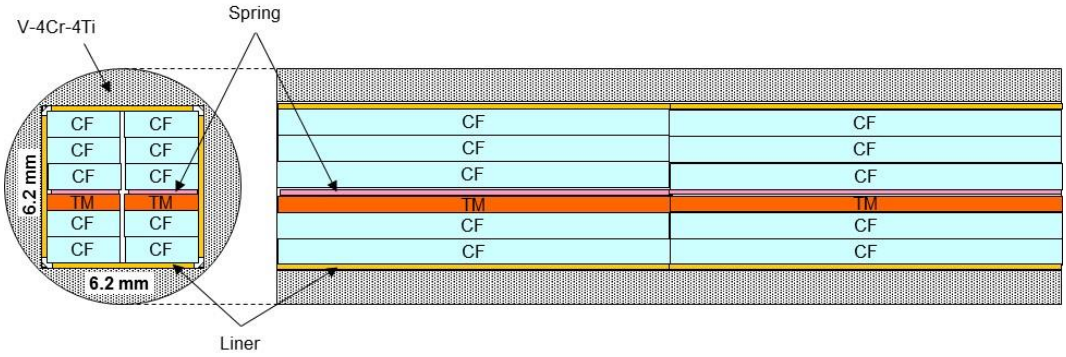

Type ID	Material	Dimensions[mm]	Qty	Main Purpose
CF	SiC/SiC	25x2.8x1	20	Flexure
TM	SiC	25x2.8x0.40	4	Thermometry
Spring	SiC	24 x 2.5 x 0.15	4	Spring
Liner	SiC	50x5.4x0.2	4	Separator

Fig. A1. Schematic illustration of SiC/SiC specimens and SiC internal components in a metallic holder.

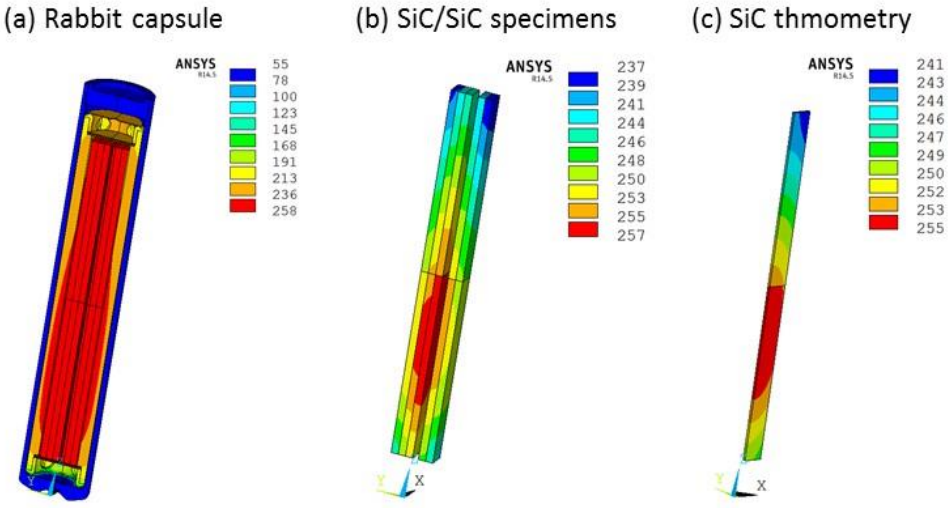

Fig. A2. Simulation of temperatures in (a) rabbit capsules, (b) SiC/SiC specimens, and (c) monolithic CVD SiC thermometer designed for irradiation experiment.

This series of high-dose irradiation experiments consisted of the irradiation of five rabbit capsules. All of the rabbits had the same capsule design. The planned target fluences were up to ~200 dpa, assuming the equivalence of 1 dpa and 1×10^{25} n/m^2 (E >0.1 MeV). The specimens were irradiated under helium atmospheres. The irradiation matrix is summarized in Table A1. The rabbit capsules were irradiated starting in High Flux Isotope Reactor cycle 457 (November 18, 2014~).

Table A1. Irradiation conditions planned for high-dose irradiation experiments

RABBIT ID	TARGET TEMP. (°C)	HFIR POSITION		FAST FLUX (n/cm^2 s)	# OF CYCLES	FAST FLUENCE PER CYCLE (n/cm^2)	TOTAL FLUENCE (n/cm^2)	TARGET DPA
SCF1	~250	TRRH	6	9.50E+14	1	1.97E+21	1.97E+21	2
SCF2	~250	TRRH	6	9.50E+14	6	1.97E+21	1.18E+22	10
SCF3	~250	TRRH	5	1.04E+15	14	2.16E+21	3.02E+22	30
SCF4	~250	TRRH	4	1.08E+15	45	2.24E+21	1.01E+23	100
SCF5	~250	TRRH	4	1.08E+15	90	2.24E+21	2.02E+23	200